nature physics

Article

https://doi.org/10.1038/s41567-022-01910-7

Light emission from strongly driven many-body systems

In the format provided by the authors and unedited

This Supplementary Information is devoted to technical derivations and complementary results and is structured as follows. We begin in Section 1 by presenting the one-dimensional single atom Hamiltonian. In Section 2, we describe the preparation protocols for inducing correlations in the atoms, based on either superradiance or spin squeezing from interatomic interactions. In Section 3, we show how permutationally invariant atomic states and operators can be described in terms of bosonic operators, in close analogy with second quantization. In Section 4, we exploit the bosonic representation of the atomic degrees of freedom to build a theory of many-body HHG in the Heisenberg picture. The ultimate achievement of such a section is the computation of the normally ordered moments $\left\langle \left(\hat{a}_n^\dagger\right)^m (\hat{a}_n)^l \right\rangle$ for each m, l, and harmonic order n. In Section 5, we show how the information on the normally ordered moments can be used to extract the Wigner function and the photon statistics of the emitted harmonics. In Section 6 with a hands-on summary outlining how to practically implement our theory in a numerical simulation. In Section 7 we present a few complementary results. In Section 8 we present an alternative phase space approach that, while not being exact, allows an efficient and qualitatively correct description of the output emission.

Note: Throughout this Supplementary Information we adopt atomic units unless otherwise specified. Moreover, we use the notations $|\Uparrow\rangle$ and $|\uparrow\uparrow\cdots\uparrow\rangle$ interchangeably (and similarly for $|\Downarrow\rangle$ and $|\downarrow\downarrow\cdots\downarrow\rangle$ and for $|\Rightarrow\rangle$ and $|\rightarrow\rightarrow\cdots\rightarrow\rangle$).

Section S1: Single-atom Hamiltonian

We describe the atoms through a one-dimensional single-particle Hamiltonian, as standard in the context of HHG [1–3].

$$\hat{h} = \frac{\hat{p}^2}{2} + V(\hat{x}), \tag{S1}$$

with $\hat{x}$ and $\hat{p}$ conjugate position and momentum operators. In the position basis, $\hat{x} = x$ and $\hat{p} = -i\partial_x$. We adopt a softened Coulomb potential [4,5], reading

$$V(x) = -\frac{1}{\sqrt{x^2 + a^2}} + V_{ab}(x), \tag{S2}$$

where we set $a = 0.816$ to match the ionization potential of Ne, that is $I_p = 0.792$, and where V_{ab} is an absorbing boundary potential to prevent nonphysical reflection of the electron form the grid boundaries [5],

$$V_{ab}(x) = \begin{cases} -5i \times 10^{-4}(|x| - x_0)^3 & if\ |x| > x_0 \\ 0 & if |x| < x_0 \end{cases}. \tag{S3}$$

The single single-particle energy eigenstates $|m\rangle$ are defined by,

$$\left(\frac{\hat{p}^2}{2} + V(\hat{x})\right)|m\rangle = w_m|m\rangle, \tag{S4}$$

with w_m the eigenenergy. Note that the complex potential V_{ab} introduces imaginary parts in the eigenstates of the free states, while having negligible effects on the bound states. The atomic spectrum is found numerically via standard space discretization. We consider a box $-L < x < L$, place the

absorbing boundaries at $\pm x_0 = \pm 0.9L$, and discretize the space with step dx. The resulting spectrum is composed of $M = \frac{2L}{dx}$ levels.

The choice of the parameters L and dx is helped by the following heuristic considerations. (i) The ponderomotive energy of the electrons is $U_p = \frac{E_0^2}{4\omega_d^2}$. We consider driving field strengths E_0 such that $U_p \gtrsim I_p \approx 0.792$, that is, $E_0 \sim 2\omega_d$. (ii) The amplitude of oscillation of a free electron under the periodic drive is $x_{max} = \frac{E_0}{\omega_d^2} \sim \frac{2}{\omega_d}$: the boundaries L should be larger than x_{max}, that is $L > \frac{2}{\omega_d}$. (iii) For free electrons in a discrete space, the discrete spectrum reads $E_k = \frac{1}{(dx)^2}\left(1 - \cos\frac{k\pi}{N_x}\right)$ for $k = 1,2,\dots,N_x$ and $N_x = \frac{2L}{dx} + 1$. On the one hand, the level spacing $\delta E \sim \frac{\pi}{2Ldx}$ should be, for a good representation of the continuum, smaller than the other energy involved scales ω_d and E_0. Thus, we set $\frac{\pi}{2Ldx} < \omega_d$, that is, $Ldx > \frac{2}{\omega_d}$. On the other hand, the largest of the levels $E_{max} = \frac{2}{(dx)^2}$ should be larger than the maximum energy of an electron under the periodic drive, that is $2U_p$, from which we ask $\frac{2}{(dx)^2} > \frac{E_0^2}{4\omega_d^2}$, that is, $dx < \sqrt{2}$. (iv) Furthermore, dx should be small enough to resolve the atomic potential. More specifically, taking the distance $\sqrt{2}a$ between the two inflection points of the potential V as its width, we need $dx < \sqrt{2}a$. This condition is more stringent than that from (iv), and therefore the one we retain. Putting all these conditions together, we require

$$dx < \sqrt{2}a, \quad L\,dx > \frac{2}{\omega_d}, \tag{S5}$$

Clearly, decreasing dx and increasing L comes at a cost, because it implies larger numbers of discrete levels ($M \approx 2L/dx$) and thus more demanding computations. All in all, we find that a good choice of parameters, for the considered $\omega_d = 0.057$ (corresponding to a wavelength of $\lambda = 800\,nm$), is $L = 150$ and $dx = 0.7$, for which the calculation involves $M = 429$ levels.

Section S2: Bosonic representation of strongly driven atoms

In this Section, we show how a general system of identical particles in a symmetrized state can be described by a set of bosonic operators associated with the single-particle states, in the same spirit of second quantization or the Schwinger mapping for angular momentum [6].

Consider a collection of N identical particles and a basis of single-particle states $\{|m\rangle\}$. Given a permutation $p = (p_1, p_2, , , p_N)$, a permutation operator $\hat{P}_p$ can be defined by

$$\hat{P}_p|m_1, m_2 \dots m_N\rangle = \left|m_{p_1}, m_{p_2} \dots m_{p_N}\right\rangle, \tag{S6}$$

where $|m_1, m_2 \dots m_N\rangle$ is the state with j^{th} particle is in state $\left|m_j\right\rangle$. A symmetrization operator creating symmetric states invariant under any permutation is then defined as

$$\hat{S} = \frac{1}{\sqrt{N!}} \sum_p \hat{P}_p\,, \tag{S7}$$

where the sum runs over all the $N!$ possible permutations p. The symmetric (Fock) state with n_1 particles in the state $|1\rangle$, n_2 in the state $|2\rangle$,…, n_m in the state $|m\rangle$ is denoted as

$$|\boldsymbol{n}\rangle = |n_1, n_2 \dots, n_m, \dots\rangle = \frac{1}{\sqrt{\prod_m n_m!}} \hat{S} \left| \underbrace{1,1,\dots,1}_{n_1 \text{times}}, \underbrace{2,2,\dots,2}_{n_2 \text{times}}, \dots, \underbrace{m,m,\dots,m}_{n_m \text{times}}, \dots \right\rangle. \quad \text{(S8)}$$

For a symmetrized state it is not important which particles are in the m^{th} level, but only how many. The factor $\sqrt{\prod_m n_m!}$ ensures the correct normalization, $\langle \boldsymbol{n}'|\boldsymbol{n}\rangle = \delta_{\boldsymbol{n},\boldsymbol{n}'}$, as can be checked with a straightaway calculation.

Consider now an operator $\hat{O} = \sum_{i=1}^{N} \hat{o}_i$ sum of identical single particle operators $\hat{o}_i$. In the chosen single particle basis, $\hat{o}_i$ reads

$$\hat{o}_i = \sum_{m,m'} O_{m',m} |m'\rangle_i \langle m|_i \,, \quad \text{(S9)}$$

with single-body matrix element $O_{m',m} = \langle m'|_i \, \hat{o}_i |m\rangle_i$. We are interested in how the many-body operator $\hat{O}$ acts on the symmetrized states $|\boldsymbol{n}\rangle$. Since $[\hat{S}, \hat{O}] = 0$, we have

$$\hat{O}|\boldsymbol{n}\rangle = \frac{1}{\sqrt{\prod_m n_m!}} \hat{S}\hat{O} | \underbrace{1,1,\dots,1}_{n_1 \text{ times}}, \underbrace{2,2,\dots,2}_{n_2 \text{ times}}, \dots, \underbrace{m,m,\dots,m}_{n_m \text{ times}}, \dots \rangle, \quad \text{(S10)}$$

and so

$$\begin{aligned} \hat{O}|\boldsymbol{n}\rangle = & \frac{1}{\sqrt{\prod_m n_m!}} \sum_m \sum_{m' \neq m} O_{m',m} \sum_{i=1}^{N} \hat{S}|m'\rangle_i \langle m|_i \left| \underbrace{1,1,\dots,1}_{n_1 \text{ times}}, \underbrace{2,2,\dots,2}_{n_2 \text{ times}}, \dots, \underbrace{m,m,\dots,m}_{n_m \text{ times}}, \dots \right\rangle \\ & + \frac{1}{\sqrt{\prod_m n_m!}} \sum_m O_{m,m} \sum_{i=1}^{N} \hat{S}|m\rangle_i \langle m|_i | \underbrace{1,1,\dots,1}_{n_1 \text{ times}}, \underbrace{2,2,\dots,2}_{n_2 \text{ times}}, \dots, \underbrace{m,m,\dots,m}_{n_m \text{ times}}, \dots \rangle, \end{aligned} \quad \text{(S11)}$$

where we split diagonal and off diagonal terms. In the rightmost sum of both, there are n_m non-vanishing terms, that is, those corresponding to the particles in state m. After the action of $\hat{S}$, these terms are all equal, and so

$$\hat{O}|\boldsymbol{n}\rangle = \frac{1}{\sqrt{\prod_m n_m!}} \sum_m \sum_{m' \neq m} O_{m',m} n_m \hat{S} | \dots, \underbrace{m,m,\dots,m}_{n_m - 1 \text{ times}}, \dots, \underbrace{m',m',\dots,m'}_{n_{m'}+1 \text{ times}}, \dots \rangle + \sum_m O_{m,m} n_m |\boldsymbol{n}\rangle \,. \quad \text{(S12)}$$

In the last expression, the first term also gives symmetrized states, but with different occupation numbers, and therefore involving a correction in the normalization

$$\hat{O}|\boldsymbol{n}\rangle = \sum_m \sum_{m' \neq m} O_{m',m} \sqrt{n_m (n_{m'} + 1)} \, |n_1, \dots, n_m - 1, \dots, n_{m'} + 1, \dots\rangle + \sum_m O_{m,m} n_m |\boldsymbol{n}\rangle \,, \quad \text{(S13)}$$

where we recognize the factors distinctive of bosonic operators. Indeed, we can formally define a pair of creation and anihilation bosonic operators $\left(b_m^\dagger, b_m\right)$ per each single-particle state $|m\rangle$, and write

$$\hat{O}|\boldsymbol{n}\rangle = \sum_{m,m'} O_{m',m} \hat{b}_{m'}^\dagger \hat{b}_m \, |\boldsymbol{n}\rangle. \quad \text{(S14)}$$

That is, calling $\hat{\boldsymbol{b}} = (\hat{b}_1; \hat{b}_2; \dots)$ the column vector of bosonic annihilation operators, and $\hat{\boldsymbol{b}}^\dagger = (\hat{b}_1^\dagger, \hat{b}_2^\dagger, \dots)$ the row vector of the bosonic creation operators, we can write

$$\hat{O} = \sum_i \hat{o}_i = \hat{\boldsymbol{b}}^\dagger \boldsymbol{O} \hat{\boldsymbol{b}}, \tag{S15}$$

where $\boldsymbol{O}$ is the matrix with single-particle entries $O_{m,n} = \langle m|_i \hat{o}_i |n\rangle_i$ (that is, a matrix of numbers). Symmetric states can be expressed in terms of bosonic operators as

$$|\boldsymbol{n}\rangle = \frac{\left(\hat{b}_1^\dagger\right)^{n_1}}{n_1!} \frac{\left(\hat{b}_2^\dagger\right)^{n_1}}{n_1!} \dots \frac{\left(\hat{b}_m^\dagger\right)^{n_m}}{n_m!} \dots |0\rangle. \tag{S16}$$

This derivation shows that, as long as the system is in the symmetrized sector, it is exactly equivalent to one of N bosons in bosonic modes $\hat{b}_m^\dagger$, associated with the single-particle states. This derivation is essentially that of second bosonization, but generalized to states of particles that are not necessarily bosons, but for which the wavefunction, Hamiltonian, and observables of interest can be considered symmetric under any permutation.

Section S3: Preparation stage

In this Section, we consider the $t < 0$ preparation stage in which correlations in the many-body atomic system are induced through interactions or superradiance. The resulting atomic state at time $t = 0$ acts as the initial condition for the subsequent HHG process. We focus on the case in which such initialization protocol only involves the single-particle ground and first excited states, $|g\rangle$ and $|e\rangle$, respectively. To describe these, we introduce standard Pauli operators $\hat{\sigma}_{x,i}$, $\hat{\sigma}_{y,i}$, and $\hat{\sigma}_{z,i}$ for the i-th atom

$$\hat{\sigma}_{x,i} = |e\rangle_i\langle g|_i + |g\rangle_i\langle e|_i; \quad \hat{\sigma}_y = \sqrt{-1}(|g\rangle_i\langle e|_i - |e\rangle_i\langle g|_i); \quad \hat{\sigma}_z = |e\rangle_i\langle e|_i - |g\rangle_i\langle g|_i. \tag{S17}$$

Collective spin operators $\hat{S}_\nu$, with $\nu = x, y, z$, read

$$\hat{S}_\nu = \sum_{i=1}^{N} \hat{\sigma}_{\nu,i} = \left(\hat{b}_1^\dagger, \hat{b}_2^\dagger\right) \sigma_\nu \begin{pmatrix} \hat{b}_1 \\ \hat{b}_2 \end{pmatrix}, \tag{S18}$$

where the (non-hatted) σ_ν denotes the standard Pauli matrices. Raising and lowering operators are also introduced as $\hat{S}^\pm = \hat{S}_x \pm i\hat{S}_y$. With this notation at hand, we can now consider two separate preparation stages, one exploiting interatomic interactions and one exploiting superradiance.

Preparation through $\pi/2$ pulse and shear force

The first protocol we consider closely follows the one introduced in the context of spin squeezing by Kitagawa and Ueda [7], exploiting one-axis twisting. The collective and undriven Hamiltonian within the two lowest levels reads

$$\hat{H} = \frac{\omega_0}{2} \hat{S}_z + \frac{\omega_J}{N} \hat{S}_z^2, \tag{S19}$$

where ω_0 is the single body energy gap between $|g\rangle$ and $|e\rangle$, whereas ω_J is an energy scale associated to the atom-atom interaction (the factor N guarantees extensivity of the Hamiltonian). First, at time $t = -t_h$, we rotate the spins with a $\pi/2$ pulse, leading them in a product state $|\Rightarrow\rangle$ in which all the spins are aligned along the direction x, $\hat{S}_x|\Rightarrow\rangle = N|\Rightarrow\rangle$. Then, we let the undriven Hamiltonian act on the system for a hold time t_h. The resulting wavefunction at time $t = 0$, that is the initial condition for HHG, reads

$$|\psi(0)\rangle = e^{-i\left(\frac{\omega_0}{2}\hat{S}_z + \frac{\omega_J}{N}\hat{S}_z^2\right)}|\Rightarrow\rangle. \tag{S20}$$

Conveniently, the time evolution operator $e^{-i\left(\frac{\omega_0}{2}\hat{S}_z + \frac{\omega_J}{N}\hat{S}_z^2\right)t_h}$ is diagonal in the chosen computational basis, which makes $|\psi(0)\rangle$ particularly easy to evaluate numerically. In Figure S1, the state $|\psi(0)\rangle$ is visualized for various hold times t_h in terms of the atomic Wigner function on the Bloch sphere.

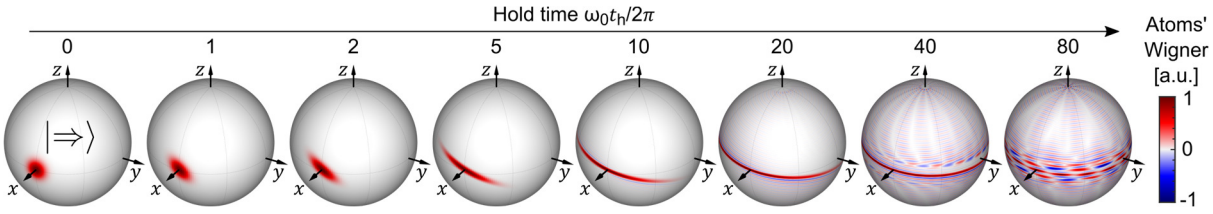

Figure S1. Preparation through one-axis twisting. The atoms can be prepared in a correlated state through interatomic $\hat{S}_z^2$ interaction. The state of the system versus time during this preparation stage is here visualized in terms of atomic Wigner function on the Bloch sphere. At time $t_h = 0$, the system is in x-polarized product state $|\Rightarrow\rangle$. The force $\hat{S}_z^2$ acts "shearing" the Wigner function, that progressively wraps around the Bloch sphere embracing its equator. At long enough times t_h, the Wigner function develops more pronounced negative parts. Here, we considered $N = 100$, $\omega_0 = 0.495$, and $\omega_J = 0.01$.

Preparation through superradiance

The second preparation protocol we consider is instead based on superradiance. First, at time $t = -t_h$ we act with a π-pulse to bring the system from the ground state $|\Downarrow\rangle$ to the excited state $|\Uparrow\rangle$. From the latter, the system then undergoes collective spontaneous emission, i.e., superradiance, that we describe with a standard Lindblad master equation [8,9] for the system's density matrix $\hat{\rho}$

$$\frac{d\hat{\rho}}{dt} = -i[\hat{H}, \hat{\rho}] + \gamma\left(\hat{S}^-\hat{\rho}\hat{S}^+ - \frac{1}{2}\{\hat{S}^+\hat{S}^-, \hat{\rho}\}\right), \tag{S21}$$

with γ the decay rate. In the considered computational basis, for the considered initial condition $\hat{\rho}(-t_h) = |\Uparrow\rangle\langle\Uparrow|$, the density matrix $\hat{\rho}$ throughout the superradiance process is diagonal. Indeed, $\hat{\rho}$ commutes with anything diagonal, and in particular with functions of $\hat{S}_z$ like $\hat{S}^+\hat{S}^- = N(N+2) - \hat{S}_z^2 + 2\hat{S}_z$. We can therefore simplify Eq. (S21) to

$$\frac{d\hat{\rho}}{dt} = \gamma\left(\hat{S}^-\hat{\rho}\hat{S}^+ - \left(N(N+2) - \hat{S}_z^2 + 2\hat{S}_z\right)\hat{\rho}\right), \tag{S22}$$

which can conveniently be solved along its diagonal only. Eq. (S22) gives the well-known magnetization and emission intensity profiles for superradiance [10]. Alternatively, in Figure S2 we illustrate the superradiance from a less common perspective, that is, by plotting the atomic Wigner function on the Bloch sphere at various times.

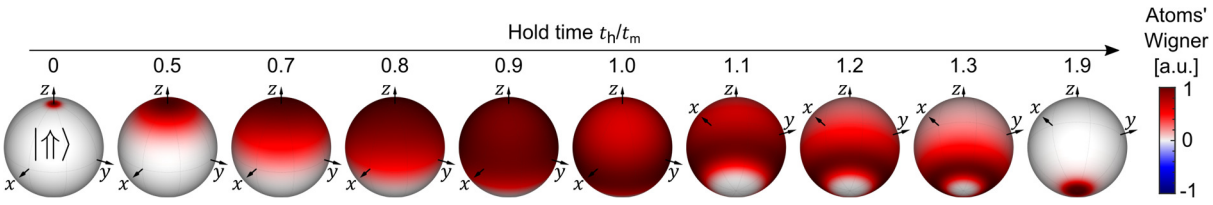

Figure S2. Preparation through superradiance. The atoms can be prepared in a correlated state through superradiance. The $t = 0$ state of the system versus time during this preparation stage is here visualized in terms of atomic Wigner function on the Bloch sphere. For vanishing hold times, that is $t_h = 0$, the system is in the product state $|\Uparrow\rangle$. For a hold time $t_h = t_m$, with t_m the time of maximum superradiant emission, the Wigner appears rather uniform on the Bloch sphere (in agreement with [10]). For a hold time $t_h \approx 1.2t_m$, the Wigner is concentrated on a ring lying between the equator and the south pole. For even longer hold times, the state of the system tends to $|\Downarrow\rangle$, and the Wigner concentrates on the South pole. Here, we considered $N = 100$ and $\gamma N = 0.1$.

Section S4: Bosonic representation of strongly driven atoms

In this Section, we apply the bosonic representation of symmetric states introduced in Section 2 to describe strongly driven atoms. Indeed, under the assumptions of our model, the system under consideration is fully symmetric, and therefore amenable to this technique. The Hamiltonian reads (in atomic units):

$$\hat{H} = \sum_{i}^{N} \hat{h}_i - \left(E_{\mathrm{c}}(t) + \hat{E}_{\mathrm{q}}\right) \sum_{i} \hat{x}_i + \sum_{\boldsymbol{k}\sigma} \omega_k \hat{a}^{\dagger}_{\boldsymbol{k}\sigma} \hat{a}_{\boldsymbol{k}\sigma}\,, \tag{S23}$$

where $\hat{h}_i$ is the one-dimensional Hamiltonian of i^{th} atom in Eq. (S1), $E_{\mathrm{c}}(t)$ is the classical time-dependent field (linearly polarized along x), and $\hat{a}_{\boldsymbol{k}\sigma}$ and $\hat{a}^{\dagger}_{\boldsymbol{k}\sigma}$ the annihilation and creation operators, respectively, of photons with wavevector $\boldsymbol{k}$ and polarization σ. The quantized field reads

$$\hat{E}_{\mathrm{q}} = \sum_{\boldsymbol{k}\sigma} \varepsilon_{\boldsymbol{k}\sigma} \left(g_{k\sigma} \hat{a}_{\boldsymbol{k}\sigma} + g^{*}_{k\sigma} \hat{a}^{\dagger}_{\boldsymbol{k}\sigma}\right), \qquad g_{k\sigma} = i\sqrt{\frac{2\pi\omega_k}{V}}, \tag{S24}$$

with $\varepsilon_{\boldsymbol{k}\sigma}$ the projection in the x direction of the polarization vector of the mode $(\boldsymbol{k}, \sigma)$ and $V \to \infty$ the volume. Using the bosonic representation in Section 2, taken with respect to the single-atom energy eigenstates $|m\rangle$ in Eq. (S4), we rewrite the Hamiltonian in Eq. (S23) as

$$\hat{H} = \hat{\boldsymbol{b}}^{\dagger} \boldsymbol{W} \hat{\boldsymbol{b}} - \left(E_{\mathrm{c}}(t) + \hat{E}_{\mathrm{q}}\right) \hat{\boldsymbol{b}}^{\dagger} \boldsymbol{D} \hat{\boldsymbol{b}} + \sum_{\boldsymbol{k}\sigma} \omega_k \hat{a}^{\dagger}_{\boldsymbol{k}\sigma} \hat{a}_{\boldsymbol{k}\sigma}\,, \tag{S25}$$

where $\boldsymbol{W}$ is a diagonal matrix of single-atom eigenenergies with entries $W_{nm} = \delta_{nm} w_n$, $\boldsymbol{D}$ is a dipole matrix with entries $D_{mn} = \langle m|\hat{x}|n\rangle$, and $\hat{\boldsymbol{b}} = (\hat{b}_1, \hat{b}_2, \ldots, \hat{b}_m, \ldots)$ is the vector of bosonic operators creating particles in the single-atom energy eigenstates.

The Heisenberg equations associated to the Hamiltonian (S25) read

$$\begin{cases} \dfrac{d\hat{\boldsymbol{b}}}{dt} = -i\boldsymbol{W}\hat{\boldsymbol{b}} + i\left(E_{\mathrm{c}}(t) + \hat{E}_{\mathrm{q}}\right)\boldsymbol{D}\hat{\boldsymbol{b}}, \\ \dfrac{d\hat{a}_{\boldsymbol{k}\sigma}}{dt} = -i\omega_k \hat{a}_{\boldsymbol{k}\sigma} + i g^{*}_{k\sigma} \varepsilon_{\boldsymbol{k}\sigma} \hat{\boldsymbol{b}}^{\dagger} \boldsymbol{D} \hat{\boldsymbol{b}}. \end{cases} \tag{S26}$$

The second equation in Eq. (S26) is readily solved by

$$\hat{a}_{\boldsymbol{k}\sigma}(t) = \hat{a}_{\boldsymbol{k}\sigma}(0) + ig^*_{k\sigma}\varepsilon_{\boldsymbol{k}\sigma}\int_{-\infty}^{t} d\tau e^{i\omega_k(\tau-t)}\widehat{\boldsymbol{b}}^\dagger(\tau)\boldsymbol{D}\widehat{\boldsymbol{b}}(\tau)\,. \tag{S27}$$

To solve the first equation, instead, we note that the quantum part of the field $\hat{E}_{\mathrm{q}}$ can in first approximation be neglected with respect to the classical strong drive $E_{\mathrm{c}}(t)$, yielding

$$\frac{d\widehat{\boldsymbol{b}}}{dt} = -i(\boldsymbol{W} - E_{\mathrm{c}}(t)\boldsymbol{D})\widehat{\boldsymbol{b}}. \tag{S28}$$

Note that neglecting the photon back-action term $\hat{E}_q$ is equivalent to neglecting superradiance. Indeed, we account for superradiance within the preparation stage (Section S3), and then we can neglect it during the strong drive pulse $E_c(t)$. Similar considerations hold for the atom-atom interactions, which are substantial during the slower preparation stage and negligible during the strong drive pulse. Eq. (S28) is linear in $\widehat{\boldsymbol{b}}$, and thus solved by

$$\widehat{\boldsymbol{b}}(t) = \boldsymbol{F}(t)\widehat{\boldsymbol{b}}(0), \tag{S30}$$

where $\widehat{\boldsymbol{b}}(0)$ is the vector of bosonic operators at time $t = 0$, when the strong pulse begins. The transition matrix is formally written as $\boldsymbol{F}(t) = T\exp\left(-i\int_0^t(\boldsymbol{W} - E_{\mathrm{c}}(\tau)\boldsymbol{D})d\tau\right)$, with T the time-ordering operator. We emphasize that, while $\widehat{\boldsymbol{b}}$ is a vector of abstract operators, each of them living in an exponentially large Hilbert space, $\boldsymbol{W}$, $\boldsymbol{D}$, and $\boldsymbol{F}(t)$ are comparably much simpler objects, namely $(M \times M)$-dimensional matrices of numbers (not operators!), that can be easily stored on a computer. These practical computational issues will be emphasized in the summary and hands-on Section 6.

Knowing the solution in Eq. (S22), the time evolution of any bilinear operator $\hat{O} = \widehat{\boldsymbol{b}}^\dagger\boldsymbol{O}\widehat{\boldsymbol{b}}$ is readily found as

$$\hat{O}(t) = \widehat{\boldsymbol{b}}^\dagger(t)\boldsymbol{O}\widehat{\boldsymbol{b}}(t) = \widehat{\boldsymbol{b}}^\dagger(0)\boldsymbol{F}^\dagger(t)\boldsymbol{O}\boldsymbol{F}(t)\widehat{\boldsymbol{b}}(0).$$

Crucially, since all the preparation procedures of the initial state we consider only involve the lowest two levels, meaning $\hat{b}_m^\dagger\hat{b}_m|\psi(0)\rangle = 0$ for any $m > 2$, we can in practice substitute $\widehat{\boldsymbol{b}}^\dagger(0) \to \left(\hat{b}_1^\dagger(0), \hat{b}_2^\dagger(0)\right)$ and $\widehat{\boldsymbol{b}}(0) \to \begin{pmatrix}\hat{b}_1(0)\\ \hat{b}_2(0)\end{pmatrix}$, which will be from now on implicit in our notation, and reduce the expression of $\hat{O}(t)$ to

$$\hat{O}(t) = \widehat{\boldsymbol{b}}^\dagger(0)\boldsymbol{o}(t)\widehat{\boldsymbol{b}}(0), \tag{S31}$$

where $\boldsymbol{o}(t)$ is the two-by-two top left corner of $\boldsymbol{F}^\dagger(t)\boldsymbol{O}\boldsymbol{F}(t)$, that is

$$\boldsymbol{o}(t) = \begin{pmatrix}\left(\boldsymbol{F}^\dagger(t)\boldsymbol{O}\boldsymbol{F}(t)\right)_{11} & \left(\boldsymbol{F}^\dagger(t)\boldsymbol{O}\boldsymbol{F}(t)\right)_{12}\\ \left(\boldsymbol{F}^\dagger(t)\boldsymbol{O}\boldsymbol{F}(t)\right)_{21} & \left(\boldsymbol{F}^\dagger(t)\boldsymbol{O}\boldsymbol{F}(t)\right)_{22}\end{pmatrix}. \tag{S32}$$

In practice, therefore, we can numerically evolve $\boldsymbol{F}(t)$ while only saving the much smaller two-by-two matrix $\boldsymbol{o}(t)$ in the computer memory, for each observable of interest. While it might be naively perceived as a somewhat "two-level matrix", $\boldsymbol{o}(t)$ contains the full many-level information on the dynamics, because obtained as a subpart of the many-level matrix $\boldsymbol{F}^\dagger(t)\boldsymbol{O}\boldsymbol{F}(t)$. The matrix $\boldsymbol{o}(t)$, which

we might call the *dynamical matrix* of the operator $\hat{O}$, is a key object in our theory. Further, we can write more explicitly

$$\hat{O}(t) = o_{11}(t)\hat{b}_1^\dagger(0)\hat{b}_1(0) + o_{12}(t)\hat{b}_1^\dagger(0)\hat{b}_2(0) + o_{21}(t)\hat{b}_2^\dagger(0)\hat{b}_1(0) + o_{22}(t)\hat{b}_2^\dagger(0)\hat{b}_2(0), \quad \text{(S33)}$$

which, exploiting $\hat{S}_\nu(0) = \widehat{\boldsymbol{b}}^\dagger(0)\sigma_\nu\widehat{\boldsymbol{b}}(0)$ and $N = \widehat{\boldsymbol{b}}^\dagger(0)\widehat{\boldsymbol{b}}(0)$, can be conveniently rewritten in terms of collective spin operators

$$\hat{O}(t) = \frac{o_{11}(t) + o_{22}(t)}{2}N + \frac{o_{22}(t,t_1) - o_{11}(t,t_1)}{2}\hat{S}_z(0) + o_{21}(t)\hat{S}^+(0) + o_{12}(t)\hat{S}^-(0). \quad \text{(S34)}$$

That is, any operator $\hat{O}(t) = \sum_i \hat{o}_i$ at time t can be written as a linear combination of standard collective spin (i.e., angular momentum) matrices, provided that the respective dynamical matrix $\boldsymbol{o}(t)$ has been computed.

Central among the observables of interest is the position, or dipole moment, $\sum_i \hat{x}_i = \widehat{\boldsymbol{b}}^\dagger \boldsymbol{D}\widehat{\boldsymbol{b}}$. We compute its two-by-two dynamical matrix $\boldsymbol{d}(t)$ as in Eq. (S32) and use Eqs. (S27) and (S31) to compactly write the time-evolved light field operators at long times (after the pulse)

$$\hat{a}_{\boldsymbol{k}\sigma} = \hat{a}_{\boldsymbol{k}\sigma}(0) + ig^*_{k\sigma}\varepsilon_{\boldsymbol{k}\sigma}\widehat{\boldsymbol{b}}^\dagger(0)\tilde{\boldsymbol{d}}(\omega_k)\widehat{\boldsymbol{b}}(0), \quad \text{(S35)}$$

where $\tilde{\boldsymbol{d}}(\omega) = \int_0^{+\infty} dt\, e^{i\omega t}\boldsymbol{d}(t)$ is the one-sided Fourier transform of the dynamical matrix of the dipole moment (thus, a ω-dependent 2×2 matrix).

The expression in Eq. (S35) can be for instance used to compute the average number of emitted photons in the frequency window $(\omega - d\omega/2, \omega + d\omega/2)$, reading

$$N_\omega = \sum_{\boldsymbol{k}\sigma:|\omega_{\boldsymbol{k}}-\omega|<\frac{d\omega}{2}} \langle \hat{a}^\dagger_{\boldsymbol{k}\sigma}\hat{a}_{\boldsymbol{k}\sigma}\rangle \approx \sum_{\boldsymbol{k}\sigma:|\omega_{\boldsymbol{k}}-\omega|<\frac{d\omega}{2}} \left\langle \varepsilon^2_{\boldsymbol{k}\sigma}\,|g_{k\sigma}|^2 \left(\widehat{\boldsymbol{b}}^\dagger(0)\tilde{\boldsymbol{d}}^\dagger(\omega_k)\widehat{\boldsymbol{b}}(0)\right)\left(\widehat{\boldsymbol{b}}^\dagger(0)\tilde{\boldsymbol{d}}(\omega_k)\widehat{\boldsymbol{b}}(0)\right)\right\rangle$$

$$\approx \frac{2}{3}\frac{\omega^3}{\pi c^3}\left\langle \sum_{i,j,k,l=1,2} \hat{b}_i^\dagger(0)\hat{b}_j(0)\hat{b}_k^\dagger(0)\hat{b}_l(0)\,\tilde{d}_{ij}{}^\dagger(\omega)\tilde{d}_{kl}(\omega)\right\rangle d\omega. \quad \text{(S36)}$$

In the last expression, we have neglected terms involving hopping to higher levels $m > 2$. Indeed, because the initial condition only involves the two lowest levels, the terms coming from $m > 2$ are negligible (being them smaller by at least a factor $1/N$ as compared to the ones that we retained). The spectrum is readily found from Eq. (S36)

$$\frac{d\epsilon}{d\omega} = \frac{\omega N_\omega}{d\omega} = \frac{2}{3}\frac{\omega^4}{\pi c^3}\left\langle \sum_{i,j,k,l=1,2} \hat{b}_i^\dagger(0)\hat{b}_j(0)\hat{b}_k^\dagger(0)\hat{b}_l(0)\,\tilde{d}_{ij}{}^\dagger(\omega)\tilde{d}_{kl}(\omega)\right\rangle. \quad \text{(S37)}$$

For instance, in the simplest scenario in which the atoms are initially all in the ground state, the dominant term in the sum is that with $i = j = k = l = 1$, yielding the familiar expression [1]

$$\frac{d\epsilon}{d\omega} = N^2\frac{2}{3}\frac{\omega^4}{\pi c^3}\left|\tilde{d}_{11}(\omega)\right|^2. \quad \text{(S38)}$$

However, the modes $a_{\boldsymbol{k}\sigma}$ in Eq. (S35) contain much more information than that on the emission spectrum. To debunk it, we want to define a mode associated with the emission into a solid angle

window $d\Omega$ of a detector, with a given polarization (for which, within $d\Omega$, we can consider $\varepsilon_{\boldsymbol{k}\sigma} \approx 1$ for one of the two polarizations, on which we focus) and within the frequency window $\left(n\omega_d - \frac{d\omega}{2}, n\omega_d + \frac{d\omega}{2}\right)$ around the n-th harmonics (Figure S3). The number of photons fulfilling these constraints can be found similarly as for Eq. (S36), and reads

$$N_n \approx d\omega \frac{d\Omega}{4\pi} \frac{(n\omega_d)^3}{\pi c^3} \left\langle \sum_{i,j,k,l=1,2} \hat{b}_i^\dagger(0)\hat{b}_j(0)\hat{b}_k^\dagger(0)\hat{b}_l(0)\, \tilde{d}_{ij}{}^\dagger(n\omega_d)\tilde{d}_{kl}(n\omega_d) \right\rangle. \tag{S39}$$

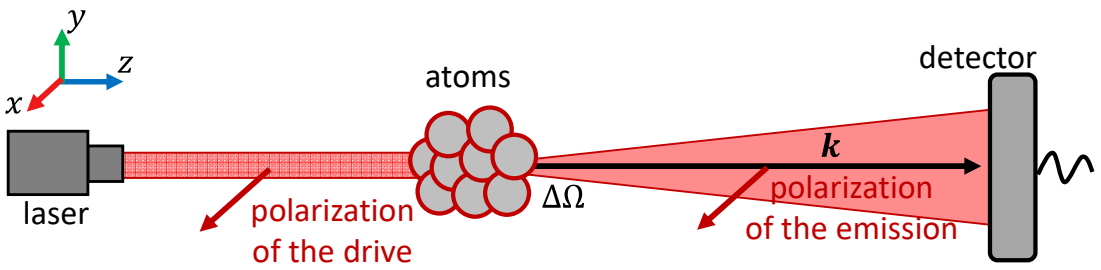

Figure S3. Schematic of the setup for HHG. We consider the polarization of the emitted light parallel to the initial driving field polarization. The emitted light is considered only within a small solid angle $\Delta\Omega$.

We can thus define a mode $\hat{a}_n$ associated to a given harmonic n as

$$\hat{a}_n = \frac{1}{\sqrt{\mathcal{N}}} \sum_{\boldsymbol{k}\in n} \hat{a}_{\boldsymbol{k}\sigma}\,, \tag{S40}$$

where the notation $\boldsymbol{k} \in n$ means that the sum runs over the modes fulfilling the selection criteria above, whereas norm is a not yet specified normalization factor. Plugging Eq. (S35) into Eq. (S40), we get

$$\hat{a}_n = \hat{a}_n(0) + \hat{\boldsymbol{b}}^\dagger(0)\boldsymbol{d}_n\hat{\boldsymbol{b}}(0), \tag{S41}$$

where we defined $\hat{a}_n(0) = \frac{1}{\sqrt{\mathcal{N}}}\sum_{\boldsymbol{k}\in n} \hat{a}_{\boldsymbol{k}\sigma}(0)$ and

$$\boldsymbol{d}_n = \frac{i}{\sqrt{\mathcal{N}}} \sum_{k\in n} g_{k\sigma}^* \tilde{d}(\omega_k)\,. \tag{S42}$$

We now choose the normalization factor $\mathcal{N}$ such that $\left[\hat{a}_n, \hat{a}_n^\dagger\right] \approx 1$. Not only does this choice render $\hat{a}_n$ a suitable photonic operator making it fulfill the standard commutation relations, but, as we will see, it also allows the correct estimate of the number of photons, which shows the consistency of this derivation. We have

$$\left[\hat{a}_n, \hat{a}_n^\dagger\right] = \frac{1}{\mathcal{N}} \sum_{k\in n}\sum_{k'\in n} \left[\hat{a}_{k\sigma}(0), \hat{a}_{k'\sigma}^\dagger(0)\right] + \hat{\boldsymbol{b}}^\dagger(0)\left[\boldsymbol{d}_n, \boldsymbol{d}_n^\dagger\right]\hat{\boldsymbol{b}}(0). \tag{S43}$$

Let us now assume a priori that the 2x2 dimensional matrix $\boldsymbol{d}_n$ has very small entries, such that $\hat{\boldsymbol{b}}^\dagger(0)\left[\boldsymbol{d}_n, \boldsymbol{d}_n^\dagger\right]\hat{\boldsymbol{b}}(0)$ can be neglected in Eq. (S36). Under this assumption, we have

$$\left[\hat{a}_n, \hat{a}_n^\dagger\right] = \frac{1}{\mathcal{N}} \sum_{k \in n} 1 \approx \frac{1}{\mathcal{N}} \frac{n^2 \omega_d^2 V d\Omega}{(2\pi)^3 c^3} d\omega, \tag{S44}$$

and, thus,

$$\mathcal{N} = \frac{n^2 \omega_d^2 V d\Omega}{(2\pi)^3 c^3} d\omega, \tag{S45}$$

and

$$\boldsymbol{d}_n \approx \sqrt{\frac{d\Omega}{4\pi} \frac{n^3 \omega_d^3}{\pi c^3} d\omega}\, \tilde{\boldsymbol{d}}(n\omega_d). \tag{S46}$$

The a priori assumption made to get from to Eq. (S43) to Eq. (S46) can now be checked as consistent. Indeed, in the relevant cases that we will consider we get from Eq. (S46) $|\boldsymbol{d}_n| \sim 10^{-4}$, so that, as long as $N \ll 10^8$, we have $\langle \hat{\boldsymbol{b}}^\dagger(0) [\boldsymbol{d}_n \boldsymbol{d}_n^\dagger] \hat{\boldsymbol{b}}(0) \rangle \ll 1$, as we assumed. As a further consistency check, we note that, computing the number of photons in the mode N_n as $\hat{a}_n^\dagger \hat{a}_n$, the same result as in Eq. (S39) is found, which comes "for free" from having enforced $\left[\hat{a}_n, \hat{a}_n^\dagger\right] \approx 1$. In our calculations, we consider $d\omega = 0.5\omega_d$ and $d\Omega = \frac{4\pi}{3}$.

Having built a suitable mode $\hat{a}_n$ for the n-th harmonc, we can now use it to extract information on the emission, accessing to its quantum features beyond the bare average number of photons. Indeed, since $\hat{a}_n(0)|0\rangle = 0$, we can compute the normally ordered moments of $\hat{a}_n$ as

$$\left\langle \left(\hat{a}_n^\dagger\right)^m (\hat{a}_n)^l \right\rangle = \left\langle \left(\left(\hat{\boldsymbol{b}}^\dagger(0) \boldsymbol{d}_n \hat{\boldsymbol{b}}(0) \right)^\dagger \right)^m \left(\hat{\boldsymbol{b}}^\dagger(0) \boldsymbol{d}_n \hat{\boldsymbol{b}}(0) \right)^l \right\rangle. \tag{S47}$$

Therefore, for the sake of computing the expectation value of normally ordered powers of $\hat{a}_n$ and $\hat{a}_n^\dagger$, the photonic operator can be written omitting the vacuum term $\hat{a}_n(0)$, thus as

$$\hat{a}_n = \frac{(d_n)_{11} + (d_n)_{22}}{2} N + \frac{(d_n)_{22} - (d_n)_{11}}{2} \hat{S}_z(0) + (d_n)_{21} \hat{S}^+(0) + (d_n)_{12} \hat{S}^-(0). \tag{S48}$$

That is, once computed the 2×2 matrix d_n (which is indeed the main computational challenge in our theory), the photonic operator $\hat{a}_n$ is just a simple linear combination of standard angular momentum operators, that can be easily represented as sparse $(N+1) \times (N+1)$ dimensional matrices on the computer (more details on the practical implementation of our theory will follow in Section 6).

Section S5: From normally ordered moments to the Wigner function and photon statistics

In this Section, we show how to exploit the information contained in the expectation value of normally ordered moments $\left\langle \left(\hat{a}^\dagger\right)^m (\hat{a})^l \right\rangle$ to compute the Wigner function and photons statistics associated to the mode $\hat{a}$ (for us, the modes of interest will then be the harmonic ones, $\hat{a}_n$).

Wigner function from moments

We begin by writing the Wigner function in terms of the Glauber function [11]

$$W(\alpha) = \frac{1}{\pi}\int P(\beta)\exp(-2|\beta-\alpha|^2)\,d^2\beta\,. \tag{S49}$$

The Glauber representation is convenient because it allows a simple expression of normally ordered moments, namely [11]

$$\langle \hat{a}^{\dagger m}\hat{a}^{l}\rangle = \int P(\beta)(\beta^*)^m\beta^l d^2\beta\,. \tag{S50}$$

The exponent in Eq. (S49) can then be expanded as

$$e^{-2|\beta-\alpha|^2} = e^{-2|\alpha|^2-2\beta\beta^*+2\beta^*\alpha+2\beta\alpha^*} = e^{-2|\alpha|^2}\sum_{l,m,k}\frac{(-1)^l 2^{l+m+k}\alpha^m\alpha^{*k}\beta^{l+k}\beta^{*l+m}}{l!\,m!\,k!}, \tag{S51}$$

that, after a couple of changes of indices, yields

$$e^{-2|\beta-\alpha|^2} = e^{-2|\alpha|^2}\sum_{l,m,k}\frac{(-1)^{l-k}2^{m+k}\alpha^{m-l}|\alpha|^{2k}\beta^l\beta^{*m}}{(l-k)!\,(m+k-l)!\,k!}. \tag{S52}$$

Plugging Eqs. (S50) and (S52) into Eq. (S49), we get

$$W(\alpha) = \frac{e^{-2|\alpha|^2}}{\pi}\sum_{l,m}(-1)^l 2^m\alpha^{m-l}\langle \hat{a}^{\dagger m}\hat{a}^{l}\rangle\left(\sum_k\frac{(-1)^k(2|\alpha|^2)^k}{(l-k)!\,(m+k-l)!\,k!}\right), \tag{S53}$$

that, by calling $\xi_{lm}(\alpha)$ all what is left apart from $\langle \hat{a}_n^{\dagger m}\hat{a}_n^{l}\rangle$, can be compactedly written as

$$W(\alpha) = \sum_{m,l}\langle \hat{a}_n^{\dagger m}\hat{a}_n^{l}\rangle\,\xi_{lm}(\alpha)\,. \tag{S54}$$

The functions $\xi_{lm}(\alpha)$ can be expressed in terms of the Kummer confluent hypergeometric function of the second kind U as

$$\xi_{lm}(\alpha) = \frac{2e^{-2|\alpha|^2}}{\pi}\alpha^{m-l}2^m\frac{U(-l,m-l+1,2|\alpha|^2)}{l!\,m!}. \tag{S55}$$

and fulfill the property $\xi_{lm}(\alpha) = \xi_{ml}(\alpha^*)$. Computing $\xi_{lm}(\alpha)$ is in general challenging: on the one hand, the sum over k in Eq. (S53) makes the calculation long, whereas on the other hand the alternating sign from the term $(-1)^k$ makes it subject to numerical cancellation. To circumvent some of these challenges, we seek to compute $\xi_{lm}(\alpha)$ by recursion. Starting from known recursion relations for the Kummer function U [12], we get

$$\xi_{lm} = -\frac{1}{\alpha l}\left(2\alpha^*\xi_{l-2,m} + (m-l+1-2|\alpha|^2)\xi_{l-1,m}\right). \tag{S56}$$

Given for $l = 0,1$ that

$$\begin{cases} \xi_{0m}(\alpha) = \xi_{m0}(\alpha^*) = \dfrac{2e^{-2|\alpha|^2}}{\pi}\dfrac{2^m\alpha^m}{m!}, \\ \xi_{1,m}(\alpha) = \xi_{m,1}(\alpha^*) = \dfrac{2e^{-2|\alpha|^2}}{\pi}\dfrac{2^m\alpha^{m-1}}{m!}(2|\alpha|^2 - m). \end{cases} \tag{S57}$$

We can therefore efficiently reconstruct by recursion all the values of ξ_{lm} and compute the Wigner function in Eq (S54).

Photon statistics from the Wigner function

With the Wigner function available, it is straightforward to obtain the full photon statistics. Indeed, the average of any operator $G(\alpha)$ [13] equals to

$$\langle G(\alpha)\rangle = \int d^2\alpha\, W(\alpha)g(\alpha)\,, \tag{S58}$$

where $g(\alpha) = \int d\mathrm{Im}[\alpha]\left\langle\sqrt{2}\mathrm{Re}[\alpha] - \mathrm{Im}[\alpha]/\sqrt{2}\middle|G(\alpha)\middle|\sqrt{2}\mathrm{Re}[\alpha] + \mathrm{Im}[\alpha]/\sqrt{2}\right\rangle e^{i\sqrt{2}\mathrm{Im}[\alpha]y}$ is the Wigner symbol associated to the operator G. The probability of observing n photons can be expressed as

$$p_n = \langle|n\rangle\langle n|\rangle, \tag{S59}$$

that is, as the expectation value of the projection operator $|n\rangle\langle n|$ onto the Fock state $|n\rangle$ with n photons. The Wigner symbol of such an operator is easily found as

$$g_n(\alpha) = 4(-1)^n e^{-2|\alpha|^2} L_n(4|\alpha|^2), \tag{S60}$$

and so the final photon statistics reads

$$p_n = \int d^2\alpha\, W(\alpha)g_n(\alpha)\,. \tag{S61}$$

Joint photon statistics and correlations between different modes

Here we propose an alternative derivation of p_n as compared to the one above. Indeed, while such alternative is numerically less stable than Eq. (S61), it has the advantage that it can be readily generalized to compute the joint probability distribution p_{nm}, that is the probability of observing n photons in a given harmonic, and m photons in a second given harmonic.

To begin with, we express the moments $\langle\hat{a}^{\dagger m}\hat{a}^m\rangle$ to the single mode photon statistics p_n (that is, the probability of observing n photons in the mode a)

$$\langle\hat{a}^{\dagger m}\hat{a}^m\rangle = \sum_{n=m}^{\infty} p_n \frac{n!}{(n-m)!}. \tag{S62}$$

We want to find the coefficients c_{lm} that reverse Eq. (S62) as

$$p_l = \sum_m c_{lm}\langle\hat{a}^{\dagger m}\hat{a}^m\rangle, \tag{S63}$$

This can be achieved substituting Eq. (S63) into Eq. (S62), from which we get the condition

$$\sum_{m=l}^{n} c_{lm} \frac{n!}{(n-m)!} = \delta_{nl}, \tag{S64}$$

with δ_{nl} the Kronecker delta. The system of linear equations (S64) is solved by

$$c_{lm} = \frac{(-1)^{m-l}}{l!\,(m-l)!}, \tag{S65}$$

that, plugged back into Eq. (S63), gives

$$p_n = \sum_{m} \frac{(-1)^{m-n}}{n!\,(m-n)!} \langle \hat{a}^{\dagger m} \hat{a}^m \rangle. \tag{S66}$$

Eq. (S61) and Eq. (S66) provide of course the same result, although we find that the former is easier to evaluate numerically, thanks to less severe involved numerical rounding errors for large number of photons.

Now let us calculate the joint probability p_{nm} to have n photons in a mode $\hat{a}_1$ and m photons in a mode $\hat{a}_2$. Generalizing Eqs. (S62) and (S63) we have

$$\left\langle \hat{a}^{\dagger k}_1 \hat{a}^k_1 \hat{a}^{\dagger l}_2 \hat{a}^l_2 \right\rangle = \sum_{n,m} p_{nm} \frac{n!}{(n-k)!} \frac{m!}{(m-l)!}, \tag{S67}$$

and

$$p_{nm} = \sum_{i,j} c_{in} c_{jm} \langle \hat{a}^{\dagger i}_1 \hat{a}^i_1 \hat{a}^{\dagger j}_2 \hat{a}^j_2 \rangle \ . \tag{S68}$$

We substitute Eq. (S68) in Eq. (S67) and get a system of linear equations in the unknowns c_{in}

$$\sum_{n} c_{in} \frac{n!}{(n-k)!} = \delta_{ik}, \qquad \sum_{m} c_{jm} \frac{m!}{(m-l)!} = \delta_{jl}. \tag{S69}$$

Solving it as for Eq. (S64), we get to the final expression

$$p_{nm} = \sum_{k,l=m}^{\infty} \frac{(-1)^{k-n}}{n!\,(k-n)!} \frac{(-1)^{l-m}}{m!\,(l-m)!} \langle \hat{a}^{\dagger k}_1 \hat{a}^k_1 \hat{a}^{\dagger l}_2 \hat{a}^l_2 \rangle . \tag{S70}$$

Section S6: Implementation oriented summary

The numerical implementation of the above theory unfolds along the following main steps, which can also serve as a summary.

1. **Single-particle spectrum**

   The first step is finding the spectrum of the single-particle Hamiltonian $\hat{h} = \frac{\hat{p}^2}{2} + V(\hat{x})$, Eq. (S4). The operators $\hat{x}$ and $\hat{p}$ are discretized and represented as $M \times M$ dimensional matrices,

with $M \approx \frac{2L}{dx}$ (e.g., $M = 429$ for the parameters considered throughout the main text). Specifically, the position basis is chosen, so that $\hat{x}$ and $\hat{p}$ are represented as a diagonal and a tridiagonal matrix, respectively. The single-particle eigenstates $|m\rangle$, with $m = 1,2,\dots,M$, are found via exact diagonalization of the discretized single atom Hamiltonian $\hat{h}$, and stored on the computer as M-components vectors. The dipole moment matrix $\boldsymbol{D}$ is build element by element, with $D_{nm} = \langle n|\hat{x}|m\rangle$, and is $M \times M$ dimensional. The diagonal matrix $\boldsymbol{W}$ of the single-particle eigenenergies is also built.

2. **Solution of the preparation stage (in Schrödinger picture)**
   The preparation stage within the two lowest atomic levels can be solved exactly. We consider the $(N+1)$-dimensional many-body Hilbert space of the symmetrized states of the two lowest single-particle eigenstates $|g\rangle$ and $|e\rangle$. Considering as a computational basis that in which $\hat{S}_z$ is diagonal, we build the $(N+1) \times (N+1)$-dimensional matrices of the collective spin operators $\hat{S}_{x,y,z}$. For the sake of more efficient computations, these operators (and the following ones) are represented as sparse matrices. We consider three different initial conditions: (i) trivial (uncorrelated) wavefunctions $|\psi(0)\rangle$, such as $|\Uparrow\rangle$, $|\Downarrow\rangle$, and $|\Rightarrow\rangle$, that can be directly represented as $(N+1)$-dimensional vectors, (ii) sheared states, obtained from Eq. (S20), (iii) states from superradiance, obtained in the form of a $(N+1) \times (N+1)$-dimensional diagonal density matrix $\hat{\rho}(0)$ by numerically integrating Eq. (S22). All these initial conditions can be represented in terms of an atomic Wigner function on a sphere [14].
3. **Integration of the HHG pulse**
   We numerically time evolve the evolution matrix $\boldsymbol{F}(t) = T \exp\left(-\frac{i}{\hbar}\int_{-\infty}^{t}(\boldsymbol{W} - E_{\mathrm{c}}(\tau)\boldsymbol{D})d\tau\right)$ in Eq. (S30). This is a $M \times M$ dimensional matrix as $\boldsymbol{W}$ and $\boldsymbol{D}$ also are (therefore, unlike the vector of bosonic operators $\widehat{\boldsymbol{b}}$, living in an abstract Hilbert space instead). This task breaks down to computing $\boldsymbol{F}(t+dt) = \exp[-i(\boldsymbol{W} - E_{\mathrm{c}}(t)\boldsymbol{D})dt]\,F(t)$, that is, the exponential of a matrix times another matrix, which can be done efficiently [15]. The full time history of $\boldsymbol{F}(t)$ is not stored in the memory: instead, we only save the 2×2 dynamical matrix $\boldsymbol{o}(t)$ for the observables of interest, and in particular, the matrix $\boldsymbol{d}(t)$ associated to the position operator, see Eqs. (S30) and (S32).
4. **Get the photonic operator for the harmonics of interest**
   Fourier transforming $\boldsymbol{d}(t)$ [Eq. (S35)] and multiplying it times the suitable coefficients [Eq. (S46)], we find the 2×2 matrix $\boldsymbol{d}_n$ for the harmonics n of interest. From this, the photonic operator associated to the harmonic, $\hat{a}_n$, is obtained as a linear combination of collective spin operators [Eq. (S48)]. By doing this, we represent the photonic operator $\hat{a}_n$ on our computer in the form of a $(N+1) \times (N+1)$-dimensional matrix. Such an operator misses the vacuum term, see Eq. (S48), under the assumption that it is only used to compute normally ordered moments.
5. **Compute normally ordered moments**
   The moments $\left\langle \hat{a}_n^{\dagger\, m}\hat{a}_n^{l}\right\rangle$ are computed for the desired initial conditions, e.g. $\left\langle \hat{a}_n^{\dagger\, m}\hat{a}_n^{l}\right\rangle = \mathrm{Tr}\left(\hat{\rho}(0)\hat{a}_n^{\dagger\, m}\hat{a}_n^{l}\right)$ in the case of preparation through superradiance, or $\left\langle \hat{a}_n^{\dagger\, m}\hat{a}_n^{l}\right\rangle = \left\langle \psi(0)\left|\hat{a}_n^{\dagger\, m}\hat{a}_n^{l}\right|\psi(0)\right\rangle$ in the case of a pure initial state $|\psi(0)\rangle$. For these operations, we keep working in the $(N+1) \times (N+1)$-dimensional Hilbert space.
6. **Compute the photonic Wigner function**
   From the normally ordered moments, we reconstruct the photonic Wigner function as in Eqs. (S54), (S56), and (S57). Note: to facilitate numerical convergence in this step, it is advised to perform a shift $\hat{a}_n \to \hat{a}_n - \langle\hat{a}_n\rangle$.
7. **Compute the photon statistics**
   From the Wigner function, we extract the photons statistics as in Eq. (S61).

Section S7: Complementary results

In this section, we report a few complementary results expanding those of the main text.

In Figures S4 and S5, we consider the same scenarios as in Figures 3 and 4 in the main text, respectively, but plot the photon statistics rather than the Wigner function. While the photon statistics contains in general les information than the Wigner function, it is on the other hand a simpler diagnostics to measure and quantify the deviations of the emitted light from a coherent state.

In Figure S6, we report the photon number statistics as in Figure 2 in the main, but adding the column corresponding to the initial condition $|\psi(0)\rangle = |\Uparrow\rangle$, that can be obtained from the ground state $|\Downarrow\rangle$ with a coherent preparation π pulse. This highlights how the number of emitted photons (that is, the efficiency of HHG) strongly depends not only on the considered harmonics, but on the atomic initial condition, too. Indeed, for $|\psi(0)\rangle = |\Uparrow\rangle$ we find, for the considered harmonics, a significantly lower number of emitted photons as compared to $|\psi(0)\rangle = |\Downarrow\rangle$, $|\Rightarrow\rangle$, and $|N/2\rangle$.

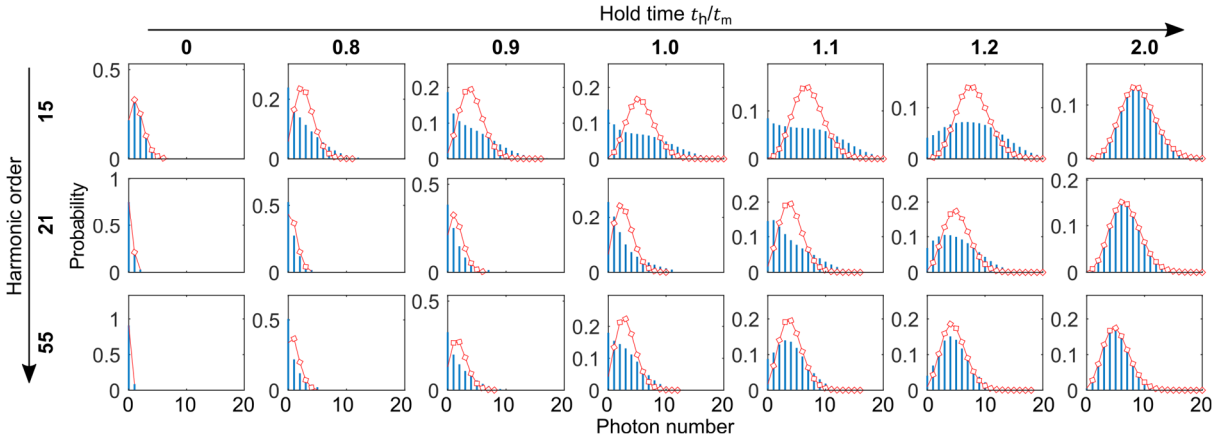

Figure S4. Photon statistics from strongly driven superradiant atoms. We consider the same scenario and parameters as in Figure 4c in the main text, but plot the photon statistics instead. To help appreciate the deviation from a coherent state, we plot for comparison a Poissonian fit in red. We observe that, for $t_h = 0$, that is for atoms initially all in their first excited state $|\psi(0)\rangle = |\Uparrow\rangle$, the emission is particularly inefficient, and fewer photons are emitted as compared, for instance, to the case of $t_h \to \infty$ (that is, ground state HHG with $|\psi(0)\rangle = |\Downarrow\rangle$).

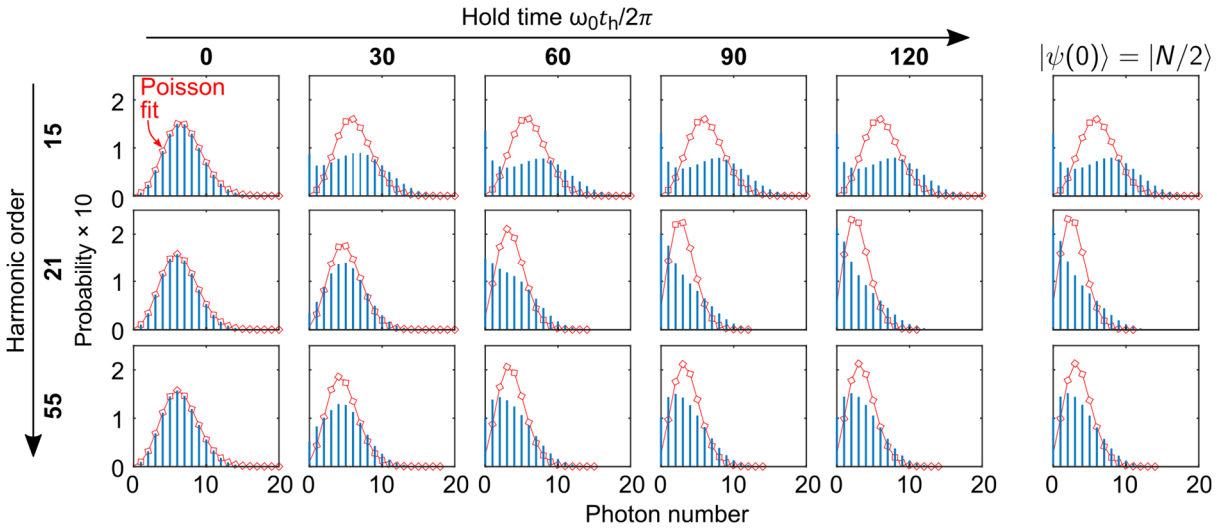

Figure S5. Photon statistics from strongly driven interacting atoms. We consider the same scenario and parameters as in Figure 3c in the main text, but plot the photon statistics instead. To help appreciate the deviation from a coherent state, we plot for comparison a Poissonian fit in red.

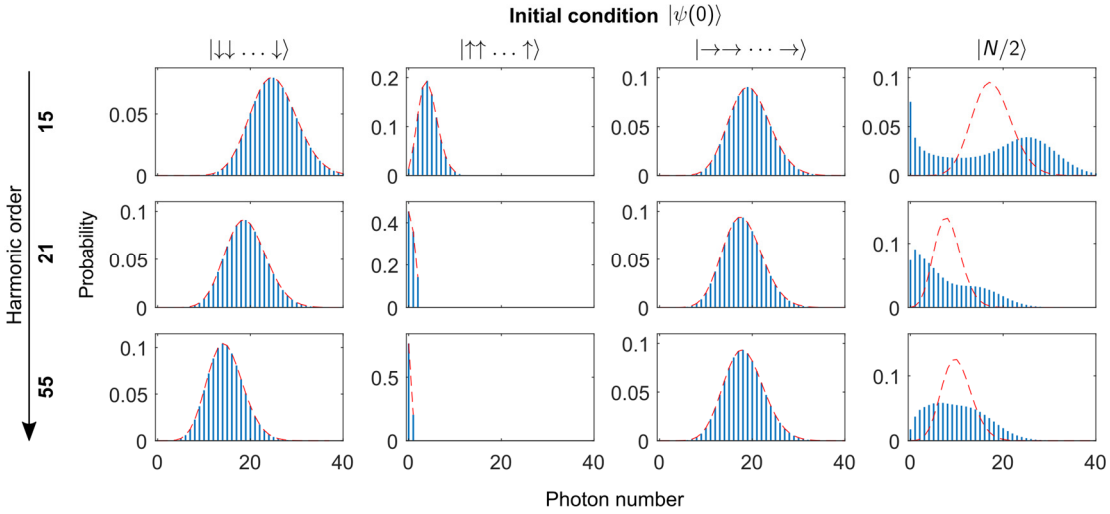

Figure S6. Dependence of the HHG efficiency on the initial condition. We plot the photon number statistics as in Figure 2 in the main text, but with an additional column (the second from left) presenting the case of an initial condition with all atoms in an excited state (marked as $|\Uparrow\rangle$). The emission from such an initial atomic state is weaker (lower photon numbers in the presented harmonics), which emphasizes the strong dependence of the HHG efficiency on the initial condition.

Section S8: Phase-space approach

In Section S4 we obtained equations describing the atoms' dynamics [Eqs. (S26) and (S28)] and the emitted radiation [Eqs. (S26) and (S27)]. The solution of these equations was provided in Eqs. (S30) and (S41), and delegates most of the numerical challenges to the computation of the transition matrix $\boldsymbol{F}$, that accounts for the single-particle atomic spectrum. These equations deal with operators, namely the bosonic operators in $\hat{\boldsymbol{b}}$ that describe the atomic system. The operatorial nature of these equations makes the statistical properties of the modes $\hat{a}_n$ rich and relatively hard to extract. In particular, obtaining the Wigner function as in Eqs. (S54-S57) is numerically rather challenging, and subject to rounding errors that become severe when the involved number of photons is large. In this Section, we propose an alternative approach based on a phase space technique that, while introducing an approximation, can be very efficient even when the involved number of photons is large (in fact, especially in this case).

S8.1: General idea

The idea of phase-space methods is to replace the Heisenberg dynamics for the operators $\hat{\boldsymbol{b}}(0)$ by an ensemble of classical trajectories for fields $\boldsymbol{\psi}(0)$. Information on quantum properties of the system (such as correlations and fluctuations) can then be extracted in terms of averages over the classical ensemble [16]. The ensemble of trajectories is obtained integrating classical equations of motion starting from an ensemble of initial conditions, that should be drawn stochastically from a distribution chosen according to the actual (single) quantum initial condition, so to mimic its intrinsic quantum fluctuations. Specifically, in our case we want to generate an ensemble of $R \gg 1$ atomic classical initial conditions $\{\boldsymbol{S}^{(r)}(0)\}$, with $r = 1,2,\dots,R$, and run the atom-photon dynamics for each of them, obtaining ensembles of classical atomic trajectories $\{\boldsymbol{S}^{(r)}(t)\}$ as well as classical photonic fields

$\left\{\alpha_n^{(r)}\right\}$ for each harmonic n of interest. From the distribution of the complex numbers $\left\{\alpha_n^{(r)}\right\}$, we can extract information on the Wigner function, photon statistics, and more. In this Section, we briefly review the fundamentals of phase-space methods, discuss how to sample the ensemble of classical initial conditions for the quantum initial conditions of interest, and show how this methods compares with the results in the main text.

Although phase-space methods have been devised for a multitude of systems [16,17], their biggest success has arguably been achieved for bosonic systems, for which the most popular method takes the name of "Truncated Wigner Approximation (TWA)". Indeed, the core idea of phase-space methods is to add quantum fluctuations on top of a leading classical dynamics, and bosonic systems have the advantage of featuring a clear notion of classical (mean-field) limit in which TWA becomes more and more accurate. This limit is that of large occupations numbers of the bosonic modes, in which complex fields $\left(\beta_j, \beta_j^*\right)$ can effectively play the role of the bosonic modes $\left(\hat{b}_j, \hat{b}_j^\dagger\right)$. The TWA for bosonic systems is a well-established technique, and its derivation, limits of validity, and applications are known [18]. For instance, it was shown in [19] that TWA leads to an error $\sim 1/\rho$, where ρ is the density of bosons in the modes. As we have shown in Section S2, the system of interest here is *effectively fully bosonic*: the photons are intrinsically bosonic, whereas the atoms can be mapped to a system of bosonic modes $\widehat{\boldsymbol{b}}$. On the one hand, if the emission is strong enough the photonic modes can eventually become highly populated. On the other hand, the first two modes $\left(\hat{b}_1, \hat{b}_1^\dagger\right)$ and $\left(\hat{b}_2, \hat{b}_2^\dagger\right)$, that we assumed to be the only ones populated at initial time and therefore the most relevant, are highly populated if $N \gg 1$. Therefore, indeed, our system of interest is well suited for treatment within a phase space method.

S8.2: Truncated Wigner Approximation – key aspects

The TWA is a method devised for dealing with the dynamics of bosons on a lattice. We shell first very quickly review it in its "traditional" form (although we refer the reader to [16,18] for thorough and more accurate reviews), and then revise it to adapt it to our system and needs.

Fundamentals of "traditional" TWA:

Quoting from [20], when dealing with bosons in a lattice, "the whole idea of the TWA is that the expectation value of any given operator Ω at time t is equal to the corresponding classical observable $\Omega_{cl}(t)$ evaluated according to standard Gross-Pitaevskii Equation (GPE) and averaged over an ensemble of initial conditions distributed according to the Wigner transform of the initial density matrix

$$\langle F(t)\rangle = \int d\psi_0^* d\psi_0 W(\psi_0, \psi_0^*) F_{cl}\big(\psi(t), \psi^*(t)\big)" \tag{S70}$$

(change of notation ours). Let us make a few remarks on Eq. (S70). Therein, $W(\psi_0, \psi_0^*)$ is the Wigner function corresponding to the (single) quantum initial condition, whereas ψ denotes a vector of complex fields, $\psi = (\psi_1, \psi_2, \dots, \psi_L)$. Specifically, the complex field $\sqrt{N}\psi_j$ is the classical variable playing the part of the bosonic mode $\hat{c}_j$ (whereas $\hat{c}_j^\dagger \to \sqrt{N}\psi_j^*$), assuming L modes in the system and N particles. For a given classical initial condition ψ_0 of the fields ψ, the classical dynamics $\psi(t)$ is obtained from the GPE, that is nothing but the classical version of the Heisenberg dynamical equation for the bosonic modes $\hat{c} = (\hat{c}_1, \hat{c}_2, \dots, \hat{c}_L)$ obtained upon replacing $\hat{c} \to \sqrt{N}\psi$. Given an observable $F = f(\hat{c}, \hat{c}^\dagger)$ that is a function of the bosonic modes, its classical counterpart is obtained replacing the modes with the

complex fields, that is, $F_{cl} = f(\psi, \psi^*)$. Note, the ambiguity on the operator ordering in f does not matter, since it falls anyway within the error $\sim 1/N$ of the method.

The integral in Eq. (S70) can be very hard to compute, especially if the number of involved modes L is large. In practice, integrals in high dimension (note, the integration variable in Eq. (S70) has dimension $2L$) can be computed with Monte Carlo methods. In essence, these methods individuate a positive definite part of the integrand, use it as a probability distribution to draw points in the high dimensional space, and compute the integral as an ensemble average over the points of the remaining part of the integrand. Unfortunately, however, no such a positive definite part appears explicitly in the integrand of Eq. (S70). In fact, what would have appeared as the most natural choice, the Wigner function W, is a *quasi*-probability and can thus take negative values. To overcome this obstacle, when adopting the TWA it is standard to replace the non-positive-definite (and normalized) quasi-probability distribution W with a positive-definite (and still normalized) probability distribution p. At the price of introducing an approximation, this allows the replacement à la Monte Carlo of the integral $\int d\psi_0^* d\psi_0 W(\psi_0, \psi_0^*)$ with an ensemble average,

$$\langle F(t) \rangle = \frac{1}{R} \sum_{r=1}^{R} F_{\mathrm{cl}} \left(\psi^{(r)}(t), \psi^{(r)*}(t) \right), \tag{S71}$$

with $\{\psi^{(r)}(t)\}$ the fields obtained from the classical (GPE) evolution of $\{\psi_0^{(r)}\}$, the ensemble of classical initial fields drawn at random according to the distribution $p(\psi_0, \psi_0^*)$, and $R \gg 1$ the number of classical trajectories (that should be taken to be large enough so to observe convergence of the results).

TWA revised:

We are now interested in understanding how a phase space method akin to TWA can be used in our setting. If on the one hand our model may appear unconventional from a condensed matter perspective (e.g., as compared to standard Bose Hubbard models [21], on the other hand it is also true that the idea of phase-space methods to describe quantum systems with an ensemble of classical trajectories is all but new in the context of quantum optics [22], and is also specifically used in the context of superradiance [9]. Using the language of TWA flashed in the previous paragraphs, our system can be fully described in terms of bosonic modes $\hat{c} = (\hat{b}_1, \hat{b}_2, \hat{a}_1, \hat{a}_3, \hat{a}_5, \dots, \hat{a}_n, \dots)$, of which the first two describe the collective atomic spin, and the remaining describe the modes of the harmonics. The respective classical complex fields are $\psi = (\beta_1, \beta_2, \alpha_1, \alpha_3, \alpha_5, \dots, a_n, \dots)$. The idea for a phase space method is then the following:

1. Generate an ensemble of classical atomic initial conditions $\{\boldsymbol{S}^{(r)}(0)\}$, with $r = 1,2, \dots, R$. This ensemble corresponds to an ensemble of bosonic fields $\{\beta_1^{(r)}(0), \beta_2^{(r)}(0)\}$ through the mapping $\boldsymbol{S} = (\beta_1, \beta_2)\boldsymbol{\sigma}\begin{pmatrix}\beta_1^* \\ \beta_2^*\end{pmatrix}$. Details on how this sampling is done will be provided in the next subsection;
2. Use Eq. (S30) to solve the classical trajectories, by just replacing $\hat{\boldsymbol{b}}(\boldsymbol{t}) \to \boldsymbol{\beta}^{(r)}(t)$ therein. In this way, we have access to the classical dynamics of all the R trajectories: $\boldsymbol{\beta}^{(r)}(t) = \boldsymbol{F}(t)\boldsymbol{\beta}^{(r)}(t)$, where the transition matrix $\boldsymbol{F}(t)$ has to be computed once and for all (and contains information on the single particle atomic spectrum, see Sections S1 and S4);

3. Plug the classical trajectories $\{\boldsymbol{\beta}^{(r)}(t)\}$ into the classical version of Eq. (S27) (in which operators are substituted by classical fields) to obtain the respective ensembles of photonic classical fields $\left\{\alpha_{\boldsymbol{k\sigma}}^{(r)}\right\}$. The same machinery of the quantum theory in Section S4 applies, leading to an ensemble of classical harmonic fields as in Eq. (7) in the main:

$$\alpha_n^{(r)} = \alpha_n^{(r)}(0) + \alpha + (\boldsymbol{u}_n + i\boldsymbol{v}_n) \cdot \boldsymbol{S}^{(r)}(0), \tag{S71}$$

In the latter, $\boldsymbol{S}^{(r)}(0)$ are the atomic initial conditions in point (1) above, whereas $\alpha_n^{(r)}(0)$ has normally distributed real and imaginary parts with standard deviation $1/\sqrt{2}$, to reflect vacuum fluctuations (indeed the Wigner function of the vacuum is $W_{vac}(X,P) = \frac{1}{\pi}e^{-X^2-P^2}$);

4. Compute an ensemble of classical photon numbers as $k_n^{(r)} = round\left(\left|\alpha_n^{(r)}\right|^2\right)$;
5. Obtain the photon statistics as the statistics of the classical photon numbers $\left\{k_n^{(r)}\right\}$.
6. Compute the classical Wigner function as a two-dimensional histogram in the complex plain of the classical fields $\left\{\alpha_n^{(r)}\right\}$. In practice, rather than computing such a histogram, we prefer to plot $\left\{\alpha_n^{(r)}\right\}$ with a scatter plot in the complex plain, imprinting the density of points in their colorcode. As an important limitation, however, the method systematically misses any possible negativity of the Wigner function.

We note that points 5 and 6 are particularly original, in the sense that TWA is normally devised to compute expectation values of some observables, rather than the photon statistics or Wigner function associated to a mode. The validity of this approach will be validated in the following by a direct comparison of the above described phase space approach and fully quantum theory.

S8.3: Sampling the classical initial conditions

We now turn to how the ensemble of initial conditions should be sampled. The goal is to find a distribution that resembles the atomic Wigner function (at time 0) as much as possible, but is positively definite.

To begin with, we compute the atomic Wigner function on the Bloch sphere for selected atomic states of interest, that is, for the state with all excited atoms $|\Uparrow\rangle$ and for that with only half of the atoms excited, $|N/2\rangle$. Both states are invariant under any permutation of the atoms, and their Wigner function $W(\theta,\phi)$ on the Bloch sphere, with θ and ϕ the polar and azimuthal angles, respectively, can be computed as in [14]. The symmetry of $|\Uparrow\rangle$ and $|N/2\rangle$ makes their Wigner $W(\theta,\phi)$ independent of the azimuthal angle ϕ, making it possible for these states to only reason in terms of quasiprobability of the polar angle θ. Considering the Jacobian factor, we call this $w(\theta) \propto |\sin\theta| W(\theta,\phi)$, and plot it in Figure S6. The goal is to replace the quasi-probability $w(\theta)$ with a positive definite probability distribution $p(\theta)$. We find that a good functional form for $p(\theta)$ is the following

$$p(\theta) \propto |\sin\theta| e^{-\frac{(\theta-\theta_0)^2}{2\sigma^2}}, \tag{S72}$$

where $\theta_0 = 0, \pi/2$ for $|\Uparrow\rangle$ and $|N/2\rangle$, respectively, and in which the width σ is found by directly fitting the quasiprobability $w(\theta)$. In the case of $|\Uparrow\rangle$ (left in Figure S7), the replacement $w(\theta) \to p(\theta)$ appears very natural and accurate, because both $w(\theta)$ and $p(\theta)$ are positive definite. In the case of $|N/2\rangle$ (center in Figure S7), $w(\theta)$ oscillates taking both positive and negative values. In this case, the replacement

with $p(\theta)$ in Eq. (S72) is motivated by the fact that the fast oscillations away from the main central peak at $\theta = \pi/2$ compensate one another in Eq. (S70) [20], and can thus be effectively neglected. In the right panel in Figure S7, by repeating the above procedure for various number of atoms N, we find that the width σ in Eq. (S72) scales with N as $\sigma = a_1 N^{-a_2}$, the coefficients a_1 and a_2 being given by a direct fit, and found to be $a_1 = 0.8887$ and $a_2 = 0.4741$ for $|\Uparrow\rangle$, and $a_1 = 0.8956$ and $a_2 = 0.9549$ for $|N/2\rangle$. By simple extrapolation, we can in this way get σ, and thus the positive definite distribution $p(\theta)$ in Eq. (S72) for any N.

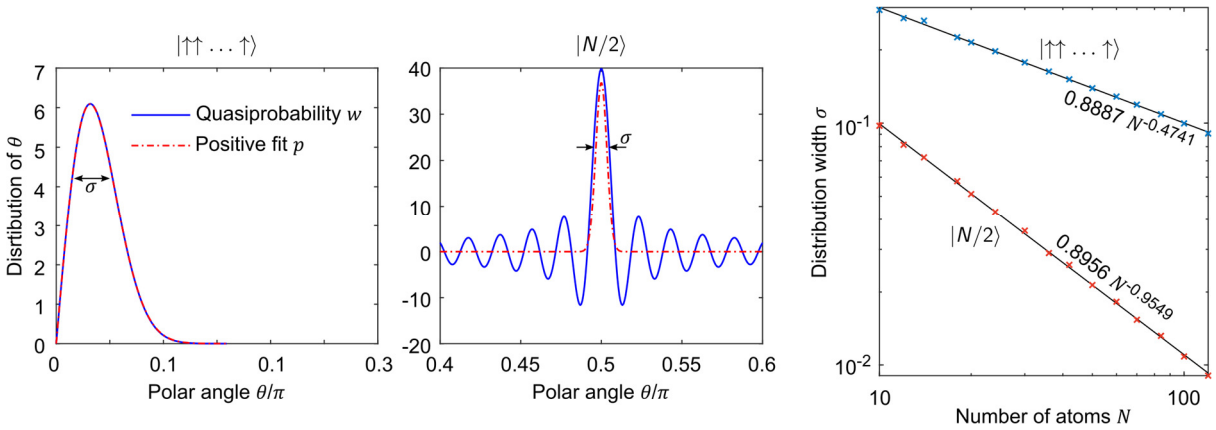

Figure S7. Analysis of the atomic Wigner function and its numerical fitting, for the cases of all-excited atoms $|\uparrow\uparrow \cdots \uparrow\rangle$ and half-excited atoms $|N/2\rangle$. For $|\uparrow\uparrow \cdots \uparrow\rangle$ and $N = 100$ (left), the Wigner function $w(\theta)$, including the Jacobian factor $\sin\theta$, is positive. For $|N/2\rangle$ and $N = 100$ (center), the Wigner function features instead a main peak at $\theta = \pi/2$ (the equator of the Bloch sphere) and rapid oscillations around it. Positive fits according to the expression in Eq. (S73) are shown in red. The fit works excellently for $|\uparrow\uparrow \cdots \uparrow\rangle$, and gets rid of the fast oscillations for $|N/2\rangle$. We find the fitting parameter σ for various system sizes N, and plot it in logarithmic scale (right) for $|\uparrow\uparrow \cdots \uparrow\rangle$ (red) and $|N/2\rangle$ (blue). This highlights a scaling $\sigma = a_1 N^{-a_2}$, with coefficients $a_{1,2}$ depending on the atomic system state ($a_{1,2}$ are found through direct interpolation).

The distribution $p(\theta)$, now at hand for any system size N and for the states $|\Uparrow\rangle$ and $|N/2\rangle$, can thus be used to sample the ensemble of classical initial conditions on the Bloch sphere according to

$$\theta^{(r)} \sim p(\theta), \qquad \phi^{(r)} = \text{randu}(0,2\pi). \tag{S73}$$

That is, $\theta^{(r)}$ is distributed according to $p(\theta)$, for which a standard rejection method can be used, whereas $\phi^{(r)}$ is distributed uniformly between 0 and 2π. Here we have discussed only the cases of $|\Uparrow\rangle$ and $|N/2\rangle$, but the discussion can be readily extended to other atomic initial conditions. For instance, the ensemble corresponding to $|\Downarrow\rangle$ can be obtained from that associated to $|\Uparrow\rangle$ by simply adding π to all the polar angles. From the ensemble of polar coordinates, we can then obtain the ensemble of points on the Bloch sphere $\{\boldsymbol{S}^{(r)}(0)\}$, and therefore that of bosonic fields $\{\boldsymbol{\beta}^{(r)}(0)\}$.

S8.4: Results

The above prescription allows us to quickly obtain information on the properties of the quantum emission. We show this by reproducing, in Figure S8, Figure 2 from the main. Indeed, the two are qualitatively very similar. While the phase space results in Figure S8 are more noisy and less precise than those in Figure 2, they are also much easier to obtain. Indeed, the computation of the Wigner function as in Figure 2 can be numerically very challenging, whereas the results in Figure S8 are

obtained by simply generating an ensemble of initial conditions and by mapping them to the complex plane of the photons (see point (3) in Section S8.2 above). Moreover, the phase space approach and Eq. (S71) in particular offer a clear insight into the shape of the Wigner function of the output harmonics. Indeed, Eq. (S71) provides a direct link between the atomic initial conditions on the Bloch sphere $\boldsymbol{S}^{(r)}(0)$ and the output photonic fields $\alpha_n^{(r)}$. The link unfolds as follows: in Eq. (S71), the term $(\boldsymbol{u}_n + i\boldsymbol{v}_n) \cdot \boldsymbol{S}^{(r)}(0)$ corresponds to a projection of the points on the sphere onto the plane individuated by the vectors $\boldsymbol{u}_n$ and $\boldsymbol{v}_n$. Such plane might also get stretched due to the angle between $\boldsymbol{u}_n$ and $\boldsymbol{v}_n$, and their different lengths. The term α represents then a shift in the complex plane, whereas $\alpha_n^{(r)}(0)$ adds a Gaussian noise to each point. With this in mind, we can therefore intuitively predict, for a given $\boldsymbol{u}_n$, $\boldsymbol{v}_n$, and initial atomic condition, the qualitative shape of the output Wigner function.

We conclude with a few remarks. First, we note that this phase space method exploits lots of the machinery used for the fully quantum theory described above and adopted in the main text. Indeed, the phase space approximation essentially only enters at the level of the final equation of the theory (Eq. (7) in the main), where the initial atomic condition is substituted by an ensemble of classical initial conditions. Therefore, in particular, the theory still exploits and requires the computation of the 2×2 dimensional matrix $\boldsymbol{d}_n$. Second, we note that the phase space method can be readily adapted to account for a preparation stage: indeed, both the protocols that we considered, that based on superradiance and that based on the interatomic interactions, can be simulated within the phase space method by just integrating the respective classical atomic dynamical equations for the each classical trajectory. Third and last, we observe that the phase space method can also provide information on the correlation between harmonics. Indeed, by computing the classical complex light fields $\left\{\alpha_n^{(r)}, \alpha_m^{(r)}\right\}$ for two harmonics n and m, and drawing them as points in the plane of, say, the real part of $\alpha_n^{(r)}$ and the imaginary part of $\alpha_m^{(r)}$, one can readily access information on the joint Wigner function of the two harmonics, which in the fully quantum treatment would be much more challenging.

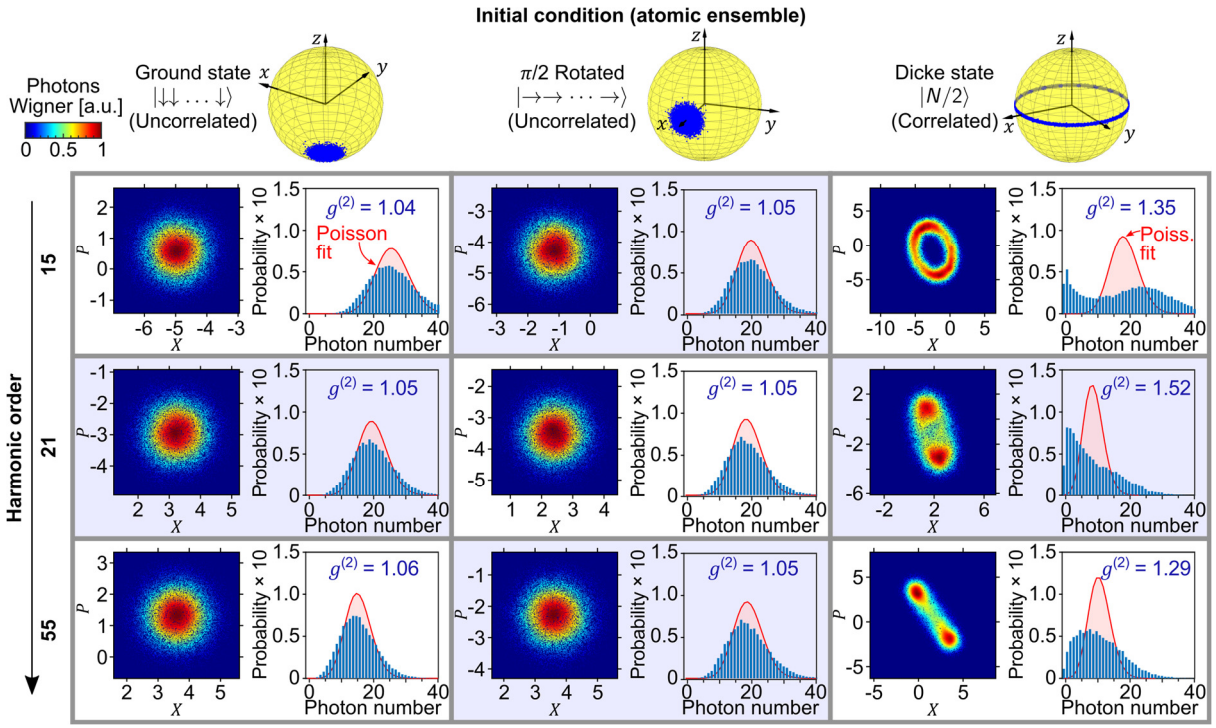

Figure S8. Many-body high-harmonic generation within a phase space method. We reproduce Figure 2 from the main within a phase space approach. The parameters considered here are the same as in Figure 2 in the main, and $R = 20000$ trajectories are considered. On top, the atomic Wigner function is replaced by a scatter plot of the atomic initial conditions on the Bloch sphere. The photonic Wigner function is instead obtained as a scatter plot of the ensemble $\{\alpha_n^{(r)}\}$ in the complex plane, the color of the dots representing their density. A good qualitative agreement of the plots with those in Figure 2 is apparent.

References

[1] M. Lewenstein, P. Balcou, M. Y. Ivanov, A. L'Huillier, and P. B. Corkum, *Theory of High-Harmonic Generation by Low-Frequency Laser Fields*, Phys. Rev. A **49**, 2117 (1994).

[2] R. W. Boyd, *Nonlinear Optics* (Academic press, 2020).

[3] C. J. Joachain, N. J. Kylstra, and R. M. Potvliege, *Atoms in Intense Laser Fields* (Cambridge University Press, 2012).

[4] L. Medišauskas, J. Wragg, H. Van Der Hart, and M. Y. Ivanov, *Generating Isolated Elliptically Polarized Attosecond Pulses Using Bichromatic Counterrotating Circularly Polarized Laser Fields*, Phys. Rev. Lett. **115**, 153001 (2015).

[5] M. E. Tzur, O. Neufeld, E. Bordo, A. Fleischer, and O. Cohen, *Selection Rules in Symmetry-Broken Systems by Symmetries in Synthetic Dimensions*, Nat. Commun. **13**, 1 (2022).

[6] H. Bruus and K. Flensberg, *Many-Body Quantum Theory in Condensed Matter Physics: An Introduction* (OUP Oxford, 2004).

[7] M. Kitagawa and M. Ueda, *Squeezed Spin States*, Phys. Rev. A **47**, 5138 (1993).

[8] H.-P. Breuer, F. Petruccione, and others, *The Theory of Open Quantum Systems* (Oxford University Press on Demand, 2002).

[9] M. Gross and S. Haroche, *Superradiance: An Essay on the Theory of Collective Spontaneous Emission*, Phys. Rep. **93**, 301 (1982).

[10] F. Bonifacio, R and Schwendimann, P and Haake, *Quantum Statistical Theory of Superradiance. II*, Phys. Rev. A **4**, 854 (1971).

[11] M. O. Scully and Z. M. S., *Quantum Optics* (Cambridge University press, 1997).

[12] M. Abramowitz and I. A. Stegun, *Handbook of Mathematical Functions with Formulas, Graphs, and Mathematical Tables*, Vol. 55 (US Government printing office, 1972).

[13] J. Garrison and R. Chiao, *Quantum Optics* (Oxford University Press, 2008).

[14] J. P. Dowling, G. S. Agarwal, and W. P. Schleich, *Wigner Distribution of a General Angular-Momentum State: Applications to a Collection of Two-Level Atoms*, Phys. Rev. A **49**, 4101 (1994).

[15] A. H. Al-Mohy and N. J. Higham, *Computing the Action of the Matrix Exponential, with an Application to Exponential Integrators*, SIAM J. Sci. Comput. **33**, 488 (2011).

[16] A. Polkovnikov, *Phase Space Representation of Quantum Dynamics*, Ann. Phys. (N. Y). **325**, 1790 (2010).

[17] J. Schachenmayer, A. Pikovski, and A. M. Rey, *Many-Body Quantum Spin Dynamics with Monte Carlo Trajectories on a Discrete Phase Space*, Phys. Rev. X **5**, 11022 (2015).

[18] A. Sinatra, C. Lobo, and Y. Castin, *The Truncated Wigner Method for Bose-Condensed Gases: Limits of Validity and Applications1*, J. Phys. B At. Mol. Opt. Phys. **35**, 3599 (2002).

[19] A. Polkovnikov, *Quantum Corrections to the Dynamics of Interacting Bosons: Beyond the Truncated Wigner Approximation*, Phys. Rev. A **68**, 53604 (2003).

[20] A. Polkovnikov, *Evolution of the Macroscopically Entangled States in Optical Lattices*, Phys. Rev. A **68**, 33609 (2003).

[21] A. Polkovnikov, S. Sachdev, and S. M. Girvin, *Nonequilibrium Gross-Pitaevskii Dynamics of Boson Lattice Models*, Phys. Rev. A **66**, 53607 (2002).

[22] C. Gardiner, P. Zoller, and P. Zoller, *Quantum Noise: A Handbook of Markovian and Non-Markovian Quantum Stochastic Methods with Applications to Quantum Optics* (Springer Science & Business Media, 2004).